Available online at www.sciencedirect.com
SCIENCE DIRECT
Polymer 46 (2005) 5040–5049
polymer
www.elsevier.com/locate/polymer

Synthesis and characterization of polyethylene-based ionomer nanocomposites

Jennifer A. Lee, Marianna Kontopoulou, J. Scott Parent*

Department of Chemical Engineering, Queen's University, Dupuis Hall, Kingston, Ont., Canada K7L 3N6

Received 16 February 2005; received in revised form 20 April 2005; accepted 21 April 2005
Available online 11 May 2005

Abstract

A solvent-free reaction of polyethylene-*g*-maleic anhydride with a tertiary amino alcohol is used to prepare an ammonium carboxylate polyampholyte (PE-*g*-PA), whose structure is characterized through spectroscopic comparisons to an appropriate model compound. The introduction of ionic functionality results in substantial increases in melt elasticity and viscosity, as well as a demonstrably improved ability to exfoliate onium ion-exchanged montmorillonite clay (NR_4^+-MM) and to disperse nanosilica (SiO_2). Physical and rheological analysis of these nanocomposites suggest that in spite of its relatively small surface area and its capacity to engage only in ion–dipole interactions with PE-*g*-PA, nanosilica provides a better balance of viscoelastic and mechanical properties when compared with onium-ion exchanged montmorillonite.

Keywords: Ionomer; Nanocomposite; Rheology

1. Introduction

The introduction of small amounts of ionic functionality to polymers of low dielectric constant can greatly affect material properties, since the polymer matrix is unable to solvate bound ion-pairs. This deficiency leads to ionic aggregation to the degree that ionomer chains are immobilized in the manner of a crosslinked material [1–6]. While physical properties may approach those of thermosetting resins, the materials retain their thermoplastic character and dissolve readily in appropriate solvents [7].

Adhesion between the polymer matrix and siliceous fillers can be enhanced by including ionomers in nanocomposite formulations, thereby facilitating melt-compounding operations that seek to exfoliate and/or disperse siliceous fillers. For example, sulfonated poly(butylene terephthalate) [8] and phosphonium salts of brominated butyl rubber [9] interact with onium-ion exchanged montmorillonite (NR_4^+-MM) with such intensity that the shear stresses imposed during compounding are transferred to the clay with a strength that is sufficient to exfoliate the material into its constituent platelets. This heightened phase adhesion is believed to result from electrostatic interactions between the charged mineral surface and the ionic functionality of the ionomer.

Our interest in polyolefin composites of onium-ion exchanged montmorillonite clay (NR_4^+-MM) centers on the development of efficient methods of generating nanocomposite structures, and the understanding of polymer–filler interactions in these systems. Our studies of maleated polyethylene (PE-*g*-MAn) composites [10,11], combined with previous work conducted on PE-*g*-MAn composites [12,13] and polypropylene (PP) composites (using PP-*g*-MAn as an in situ compatibilzer) [14–17], have demonstrated the limited capacity of polyolefins to exfoliate NR_4^+-MM by a melt-compounding approach. Typically, maleated polyolefin/NR_4^+-MM composites are hybrid materials that contain a mixture exfoliated platelets, intercalated tactoids, and native clay particles. Since exfoliation is required to transform the mineral into a reinforcing filler, this failure to delaminate the clay and disperse its constituent platelets results in a loss of reinforcement potential.

The present work is concerned with the synthesis of a polyampholyte (PA) derivative of polyethylene and the

* Corresponding author. Tel.: +1 613 533 6266; fax: +1 613 533 6637.
E-mail address: parent@chee.queensu.ca (J.S. Parent).

0032-3861/$ - see front matter © 2005 Elsevier Ltd. All rights reserved.
doi:10.1016/j.polymer.2005.04.044

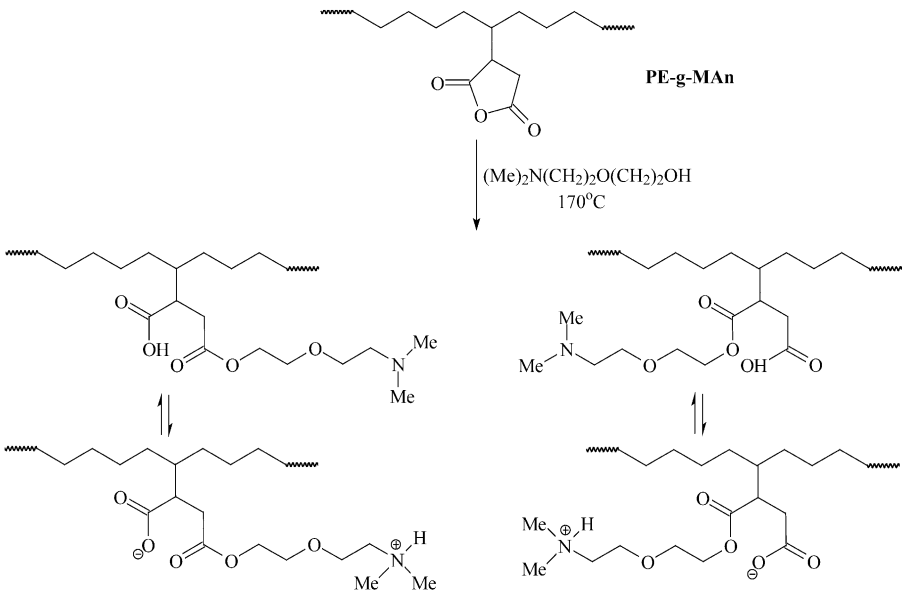

Scheme 1.

interactions of this ionomer with siliceous fillers. The reaction of PE-*g*-MAn with a tertiary amino alcohol is used to generate a zwitterionic derivative, PE-*g*-PA (Scheme 1) that, in theory, is equipped to interact directly with the anionic surface of NR_4^+-MM by displacing onium ion from the mineral. In this respect, PE-*g*-PA differs from conventional metal carboxylate salts in that both anionic and cationic functionality are bound covalently to the polymer backbone. The interaction between a PE-*g*-PA matrix and nano-scale silica is also of interest, given the propensity of high-surface energy silica fillers to agglomerate when compounded with non-polar materials. This agglomeration tendency can be overcome by lowering the surface energy of the filler using surface treatments, or by employing appropriate coupling agents [18]. Our objective was to achieve nanosilica dispersion without compromising the surface activity of the filler, and without need for expensive reagents.

This report presents details regarding the synthesis and rheology of PE-*g*-PA, along with a careful examination of the properties of ionomer nanocomposites prepared from NR_4^+-MM and nanosilica. The polyampholyte structure is characterized unambiguously through comparisons of spectroscopic data with that of analogous model compounds, and the ionic nature of the network is verified by rheological and solubility studies. The ability of PE-*g*-PA to exfoliate NR_4^+-MM clay and disperse nanosilica is assessed, and the influence of these fillers on melt rheology and mechanical properties is examined.

2. Experimental

2.1. Materials

Montmorillonite clay was used as supplied (Nanomer® I.44PA (NR_4^+-MM), Nanocor Inc., Arlington Heights, Illinois; ion-exchanged with dimethyldialkylammonium halide (70% C_{18}, 26% C_{16} and 4% C_{14})). Fumed amorphous silicon dioxide with a measured specific surface area of 200 m^2/g was used as supplied (Aerosil® 200 (SiO_2), Degussa Corp., Parsippany, New Jersey). Maleated high-density polyethylene containing approximately 1 wt% of pendant succinic anhydride groups was obtained from DuPont Canada (PE-*g*-MAn, Fusabond® M611-25, MFI = 9.6). 2,6-Di-*tert*-butyl-4-methylphenol (BHT, 99%+), 2-[2-(dimethylamino)ethoxy]ethanol (DMAEE, 98%), (2-dodecen-1-yl)-succinic anhydride (DDSA, 95%), pyridine, ethyl chloroformate, 1-hexanol were used as received from Sigma-Aldrich (Oakville, Ontario). The initiator 2,5-dimethyl-2,5-di(*t*-butylperoxy)hex-3-yne (Lupersox® 130 (L-130), 90%, ATOFINA Chemicals, Inc., Philadelphia, Pennsylvania), and the antioxidant 2,2-methylene-bis(4-methyl-6-*tert*-butyl)phenol (Cyanox® 2246®, CYTEC Industries Inc., West Paterson, New Jersey) were used as supplied. All solvents used were of reagent grade and obtained from Fisher Scientific Ltd (Ottawa, Ontario).

2.2. Synthesis of (5E)-3-({2-[2-(dimethylammonio)ethyoxy]ethoxy}carbonyl)pentadec-5-enoate and (4E)-2-(2-{2-[2-(dimethylammonio)ethoxy]ethoxy}-2-oxoethyl)tetradec-4-enoate

DDSA (0.22 g, 0.81 mmol) and DMAEE (0.11 g, 0.81 mmol) were heated to 80 °C for 30 min, yielding a clear yellow viscous liquid. MS analysis; required for $C_{22}H_{41}NO_5^+$ *m/e* 399.6, found 399.3. ^{1}H NMR ($CDCl_3$): δ 0.86 (t, 3H, $-CH_3$), 1.18–1.37 (m, 14.4H, $-CH_2-$), 1.96 (m, 2.18H, $-CH_2-CH=CH$), 2.06–2.31 (m, 1.24H, –CH–CH=CH), 2.32–2.48 (m, 2.02H, 1×–CH–CH=CH, 1×–CH–C=O), 2.52 (m, 1.34H, –CH–C=O), 2.61 (d,

3.87H, CH_3–NH), 2.75 (s, 2.28H, CH_3–NH), 2.84 (m, 0.37H, –CH–C(=O)O^-), 2.94 (m, 1.25H, –CH–NH), 3.09 (t, 0.63H, –CH–NH), 3.57 (t, 0.70H, –CH–O), 3.62 (m, 1.09H, –CH–O), 3.69 (m, 1.86H, 2×–CH–O), 3.75 (t, 0.64H, –CH–O), 4.25 (m, 1.28H, –CH–O), 5.33 (m, 1.12H, =C=H), 5.43 (m, 1.02H, =C–H), 7.67 (bs, 3.26H, –OH). FT-IR: 3590–3170 cm^{-1} (w/br, ν_s O–H); 1732 cm^{-1} (s, ν_s C=O); 1577 cm^{-1} (m, ν_{as} CO_2^-); 1387 cm^{-1} (w, ν_s CO_2^- and δ_s O–H); 1166 cm^{-1} (m, ν_s C–C=O–O).

2.3. Quantitative dehydration of succinic acid moities within PE-g-MAn

PE-*g*-MAn (5 g), pyridine (1 ml) and xylene (100 ml) were heated to reflux under a nitrogen atmosphere prior to the addition of a solution containing xylene (10 ml) and ethyl chloroformate (1 ml). The solution was refluxed for 30 min before recovering the dehydrated polymer by precipitation with acetone (300 ml). The product was rinsed with acetone and dried under vacuum. FT-IR: 1866 cm^{-1} (w, ν_s and ν_{as} C=O); 1790 cm^{-1} (s, ν_s and ν_{as} C=O).

2.4. Quantitative transformation of PE-g-MAn to PE-g-PA

Dehydrated PE-*g*-MAn (0.5 g) was mixed with DMAEE (0.0195 g, 0.1464 mmol) at 170 °C for 10 min in an Atlas laboratory mixing moulder. FT-IR: 1738 cm^{-1} (s, ν_s C=O); 1641 cm^{-1} (w/br, ν_{as} CO_2^-); 1586 cm^{-1} (w/br, ν_{as} CO_2^-).

2.5. Melt-state preparation of PE-g-PA

PE-*g*-MAn (40 g) was partially dehydrated by heating to 170 °C for 20 min with BHT (0.02 g, 0.09076 mmoles) in a Haake PolyLab torque rheometer that controlled a Rheomix 610p mixing chamber equipped with roller rotors. DMAEE (0.5966 g, 4.4793 mmol) was added to the chamber, and mixing was continued at 170 °C for 5 min. FT-IR: 1864 cm^{-1} (w, ν_s and ν_{as} C=O); 1790 cm^{-1} (m, ν_s and ν_{as} C=O); 1735 cm^{-1} (s, ν_s C=O); 1710 cm^{-1} (s, ν_s C=O); 1641 cm^{-1} (w/br, ν_{as} CO_2^-); 1585 cm^{-1} (w/br, ν_{as} CO_2^-). T_m = 134 °C.

2.6. Peroxide-mediated crosslinking of PE-g-MAn

PE-*g*-MAn (35 g) was mixed with L-130 (0.0364 g, 0.12 mmol) at 140 °C and 60 rpm for 7 min in a Haake PolyLab torque rheometer. Peroxide-mediated crosslinking of this masterbatch was conducted in the cavity of an Alpha Technologies Advanced Polymer Analyzer (APA 2000) at 180 °C for 18 min (corresponding to five half-lives of the initiator). The rheological properties of the crosslinked product were characterized immediately in the instrument at 150 °C.

2.7. Gel content analysis

Gel content measurements on PE-*g*-PA and the peroxide-crosslinked PE-*g*-MAn were performed in accordance with ASTM D2765. Samples were extracted with xylene or with a 7 wt% solution of hexanol in xylene for 12 h and dried at 130 °C under vacuum to constant weight. All extraction mixtures were stabilized using Cyanox® 2246® (0.003 g, 0.01 mmol) to prevent oxidative crosslinking.

2.8. Composite preparation

PE-*g*-PA composites were prepared the same manner as for the melt-state PE-*g*-PA, with subsequent addition of the designated amount of NR_4^+-MM or SiO_2, after which the material was mixed for a further 7 min.

2.9. Analysis

FT-IR spectra were acquired on thin polymer films using a Nicolet Avatar 360 E.S.P. spectrometer at a resolution of 4 cm^{-1}. NMR spectra were recorded with a Bruker Avance-600 spectrometer (600.17 MHz ^{1}H, 150.92 MHz ^{13}C) in deuterated chloroform ($CDCl_3$) with chemical shifts referenced to tetramethylsilane (TMS). Mass spectra were recorded on a Waters ZQ single quadrupole mass spectrometer in a 1:1 solution of nitromethane and dichloromethane using electrospray ionization. Thermal properties were measured using a TA Instruments Q100 differential scanning calorimeter. Thermal history was erased by heating to 200 °C at a rate of 10 °C/min. The sample was then cooled to −85 °C at 5 °C/min and then heated to 200 °C at 10 °C/min. The melting temperature was determined from the second heating cycle.

2.10. Wide-angle X-ray diffraction

Wide-angle X-ray diffraction (WAXS) analyses of NR_4^+-MM composites were conducted with a Scintag Model X1 diffractometer (Cu K_α radiation λ = 1.5406 Å, generator voltage = 45 kV, current = 40 mA). Samples were pressed films approximately 400 μm thick and were scanned in 2θ ranges from 1–30° at a rate of 1 °/min. Measurements were recorded every 0.02°. For comparative purposes, the WAXS patterns were normalized using the intensity of the strongest reflection.

2.11. Transmission electron microscopy

TEM samples were sectioned with a diamond knife on a Leica Ultracut cryoultramicrotome to approximately 70 nm thick at −100 °C and placed on formvar coated copper grids. Images were recorded using a FEI Tecnai 20 transmission electron microscope (TEM) operated at 200 kV and equipped with a Gatan Dualview digital camera.

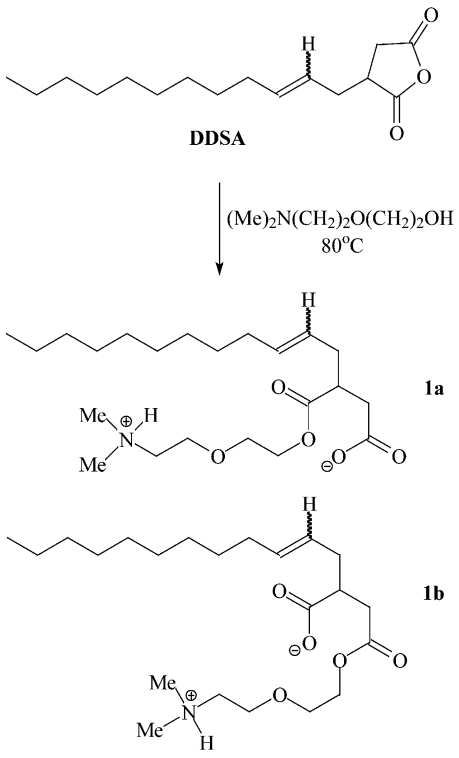

Scheme 2.

2.12. Rheological characterization

The viscoelastic properties (G', G'' and η^*) of PE-*g*-PA and its composites were measured as a function of angular frequency (ω) from 0.03 to 31 rad/s using an Alpha Technologies Advanced Polymer Analyzer 2000 (APA 2000) oscillatory rheometer operated using the biconical die configuration at a temperature of 150 °C. In the case of PE-*g*-MAn, its rheological properties were measured as a function of angular frequency (ω) from 0.04 to 188 rad/s using a Reologica ViscoTech controlled stress rheometer with 20 mm diameter parallel plates operated in the oscillatory mode at a gap of 1.5 mm and temperature of 150 °C. Stress or strain sweeps verified that all data were acquired within the linear viscoelastic regime.

Dynamic oscillatory measurements of PE-*g*-PA and PE-*g*-MAn were measured from 150 to 170 °C and 150 to 210 °C, respectively, in 10 °C intervals. Mastercurves of the elastic (G') and viscous (G'') moduli were constructed for each material by shifting the curves to the curve obtained at a reference temperature of 150 °C. The resulting horizontal shift factors obtained from the superposition process were fitted to an Arrhenius-type equation, yielding an estimate of the flow activation energy [19].

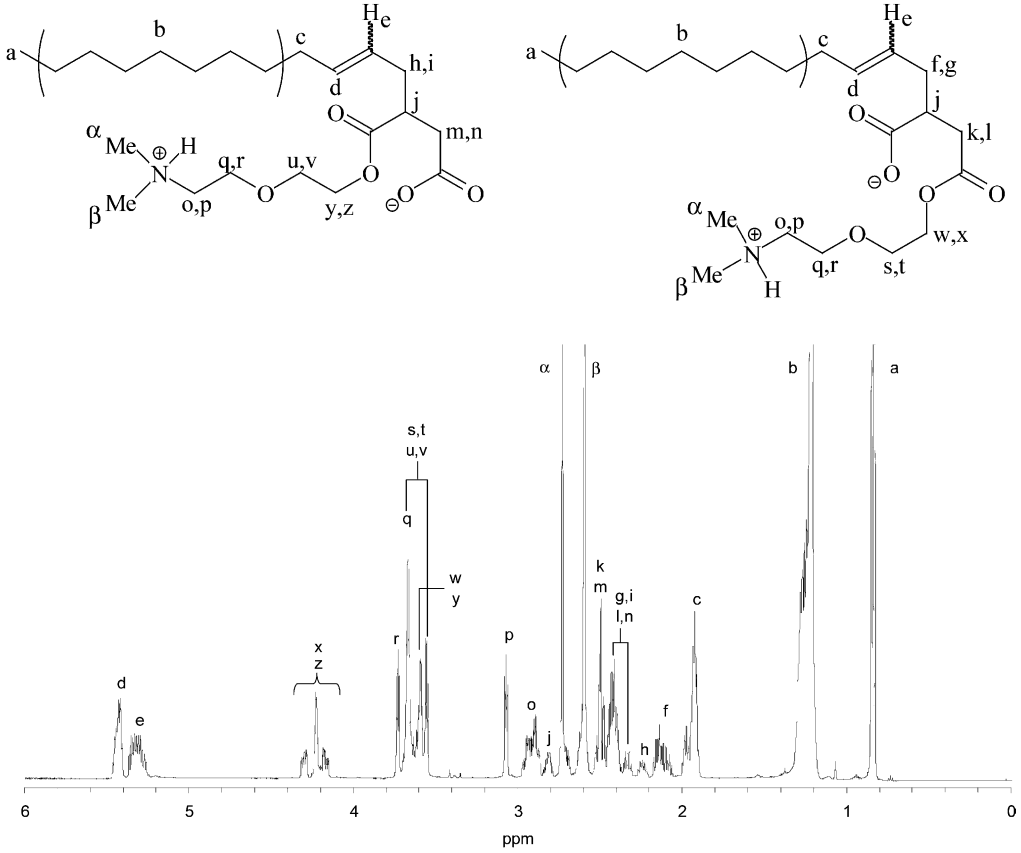

Fig. 1. ^{1}H NMR spectra of DDSA-*g*-PA in $CDCl_3$ (TMS as internal standard).

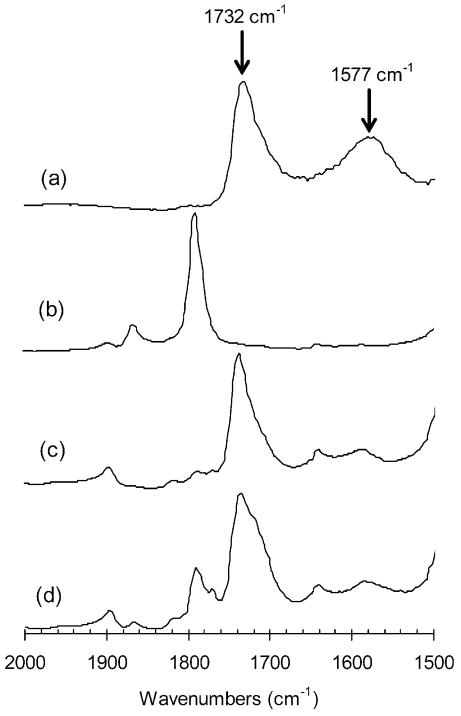

Fig. 2. FT-IR spectra of (a) DDSA-*g*-PA, (b) dehydrated PE-*g*-MAn, (c) PE-*g*-PA, (d) PE-*g*-PA (melt compounded).

2.13. Tensile testing

An Instron Series 3369 universal testing instrument operated at a crosshead speed of 50 mm/min and at room temperature was used to measure the tensile properties of the composites according to ASTM D638. Samples were prepared by compression moulding sheets 1.5 mm in thickness at approximately 180 °C from which test specimens were cut using a Type V die. A minimum of 10 specimens for each PE-*g*-PA composite composition were tested in order to estimate the precision of the reported data.

3. Results and discussion

3.1. Synthesis and characterization of PE-g-PA

A simple and efficient method of preparing a polyampholyte derivative of polyethylene exploits the reactivity of anhydrides with respect to tertiary amino alcohols (Scheme 1). Ring-opening by the alcohol is rapid and irreversible, and a subsequent proton transfer generates the desired secondary ammonium carboxylate salt. These transformations are well-illustrated by the reaction of 2-[2-(dimethylamino)ethoxy]ethanol (DMAEE) with (2-dodecen-1-yl)-succinic anhydride (DDSA) to yield products that can be characterized unambiguously (Scheme 2). The ^{1}H NMR spectrum shown in Fig. 1 provides evidence of two positional isomers, whose structural assignments have been made on the basis of two-dimensional COSY, HMBC and

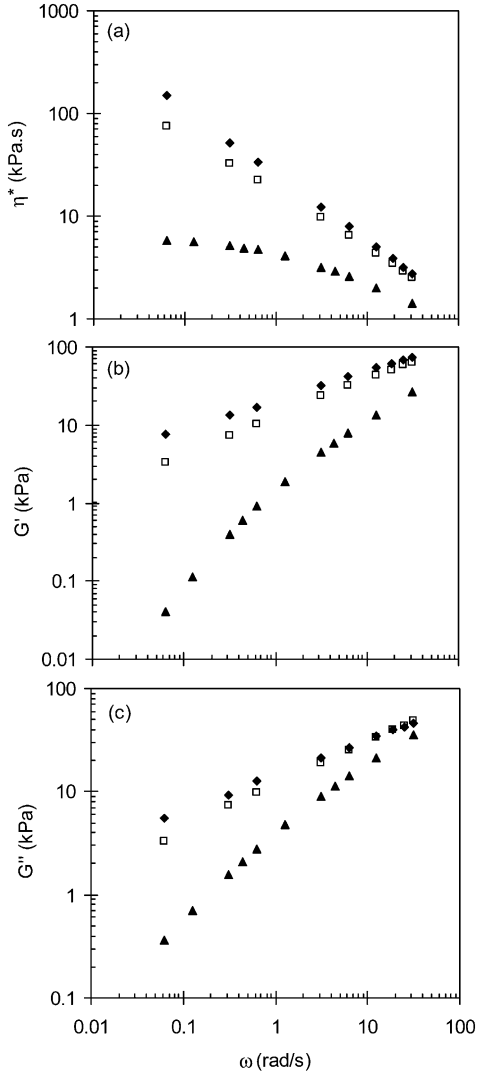

Fig. 3. (a) Complex viscosity (η^*), (b) elastic modulus (G'), and (c) viscous modulus (G'') as a function of frequency (ω) at 150 °C where, ▲ PE-*g*-MAn, ◆ PE-*g*-PA, □ 0.1 wt% L-130/PE-*g*-MAn.

HSQC NMR experiments. These assignments are further supported by characteristic FT-IR absorbances of ester (1732 cm^{-1}) and carboxylate anion (1577 cm^{-1}) functionality, as revealed in Fig. 2(a).

The yield of the desired ammonium carboxylate salt derived from PE-*g*-MAn is dependent on the state of grafted monomer. Due to the moisture sensitivity of anhydrides, PE-*g*-MAn contains a high proportion of succinic acid functionality [20], whose reaction with DMAEE generates a carboxylate salt in which the ammonium ion is not bound to the polymer backbone. Complications derived from diacid functionality can be overcome by dehydrating the material in solution by treatment with ethyl chloroformate and pyridine. The product of this treatment contains only anhydride functionality, as evidenced by the FT-IR spectrum shown in Fig. 2(b). Immediate exposure of dehydrated PE-*g*-MAn to DMAEE yields the desired polyampholyte functionality, as revealed by a comparison

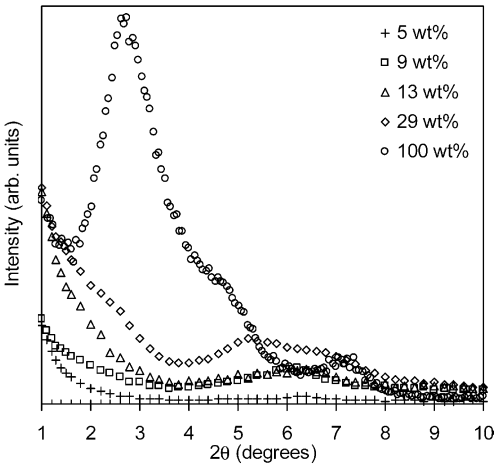

Fig. 4. WAXS diffraction patterns of NR_4^+-MM and its PE-*g*-PA composites.

of the FT-IR spectrum of the PE-*g*-PA product (Fig. 2(c)) with that derived from the model compound (Fig. 2(a)). Both spectra contain an intense absorbance at 1732 cm^{-1} that is characteristic of an ester, along with the expected resonance at 1577 cm^{-1} derived from the carboxylate ion. The breadth of these signals can be attributed to the existence of positional isomers, and to the inherent broadness of carboxylate anion resonances due to hydrogen bonding effects [21].

Although quantitative dehydration of PE-*g*-MAn improves the yield of polyampholyte functionality, it is impractical when applied to the large-scale preparations demanded by melt compounding operations. Fortunately, a high degree of dehydration can be accomplished by heating the material in conventional polymer processing equipment. By maintaining PE-*g*-MAn at 170 °C for 20 min, a molar ratio of anhydride to diacid functionality of approximately 90:10 is achieved, and the subsequent addition of DMAEE to the system results in a high yield of the desired zwitterion. The FT-IR spectrum for PE-*g*-PA prepared by this technique (Fig. 2(d)) reveals a large proportion of the desired ester, along with small amounts of residual anhydride and diacid functionality. Since this material could be prepared with good efficiency and on a large scale, it was used throughout the following studies of melt rheology and nanocomposite properties.

3.2. Rheological properties of PE-g-PA

The effect of ionic functionality on the rheological properties of non-polar polymers is well understood [1–6], and the results of transforming PE-*g*-MAn into PE-*g*-PA are consistent with those observed for other ionomer systems (Fig. 3). The polyampholyte displayed an order of magnitude increase in complex viscosity (η^*) and storage modulus (G'), and all evidence of a Newtonian plateau was lost. Moreover, we did not observe any time-dependence of the rheological properties of PE-*g*-PA, unlike the non-ionic parent material PE-*g*-MAn, which has been shown to build melt viscosity when analyzed under low shear stress conditions [11].

Further insight into the effect of ionic aggregation on

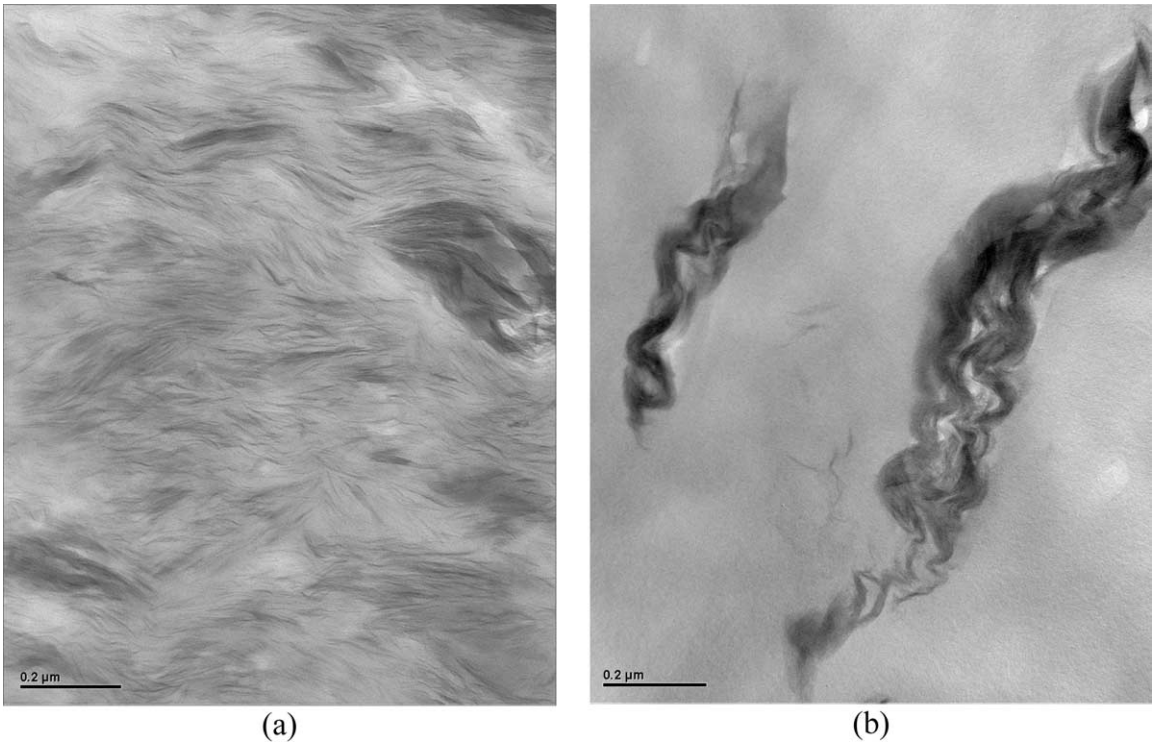

Fig. 5. TEM images of (a) 40 wt% NR_4^+-MM/PE-*g*-PA, (b) 5 wt% NR_4^+-MM/HDPE (scale bars correspond to 0.2 μm).

melt viscosity is gained by applying the time-temperature superposition principle to estimate an activation energy for polymer flow [22]. Since this technique has been applied successfully to ionomers containing low ion-pair concentrations, it is expected to be valid for the PE-*g*-PA system of interest [23]. The horizontal shift factors obtained from the superposition of the G' and G'' curves were fitted to an Arrhenius-type equation, yielding an activation energy for viscous flow of 159 kJ/mol for PE-*g*-PA, compared to just 37 kJ/mol for PE-*g*-MAn. The considerable difference in these values reflects the restriction of polymer chain mobility in the melt-state due to a network effect arising from ion-pair aggregation [6].

To provide a basis for evaluating network effects in polyethylene melt rheology, and to verify that the source of elasticity in PE-*g*-PA was ionic aggregation, we prepared a thermoset derivative of PE-*g*-MAn. The result of activating 0.1 wt% of 2,5-dimethyl-2,5-di(*t*-butylperoxy)hex-3-yne (L-130) within PE-*g*-MAn is illustrated in Fig. 3. This peroxide cure raised the complex viscosity and elasticity of the polymer, and eliminated its Newtonian plateau. All attempts to dissolve samples of thermoset PE-*g*-MAn were unsuccessful, as the material could only be swelled by xylenes and hexanol/xylene mixtures.

We found that PE-*g*-PA was similarly insoluble in boiling xylene (99% gel), but the polyampholyte was completely soluble in a mixture containing 7 wt% hexanol in xylene. The effect of small amounts of polar co-solvents on the solubility of ionomers is well documented [7], and our observations confirm that the polymer network established within PE-*g*-PA is derived from aggregation of the ammonium carboxylate functionality.

3.3. NR_4^+-MM ionomer composites

The objective of melt-compounding an onium-ion exchanged clay into a polyolefin is to enhance the reinforcement capacity of the filler by delaminating the mineral and dispersing its constituent platelets. Toward this end, we have compounded PE-*g*-PA with NR_4^+-MM, and analyzed the resulting composites by WAXS and TEM. Fig. 4 shows the WAXS diffraction patterns for NR_4^+-MM/PE-*g*-PA composites containing various amounts of the mineral. None of the composites generated the (001) diffraction peak that is characteristic of the exchanged clay's interlayer spacing, which indicates that the ordered structure of the layered mineral was effectively eliminated. This complete disruption of the clay's native structure was observed for filler loadings as high as 30 wt%, which is remarkable given that a previously reported WAXS analysis of a corresponding PE-*g*-MAn composite containing just 5 wt% of NR_4^+-MM retained a significant (001) diffraction peak [10,11]. The origin of a weak diffraction signal centered at $2\theta = 6$ is not known precisely, but it may arise from a small population of residual sodium montmorillonite within the NR_4^+-MM clay used throughout this work.

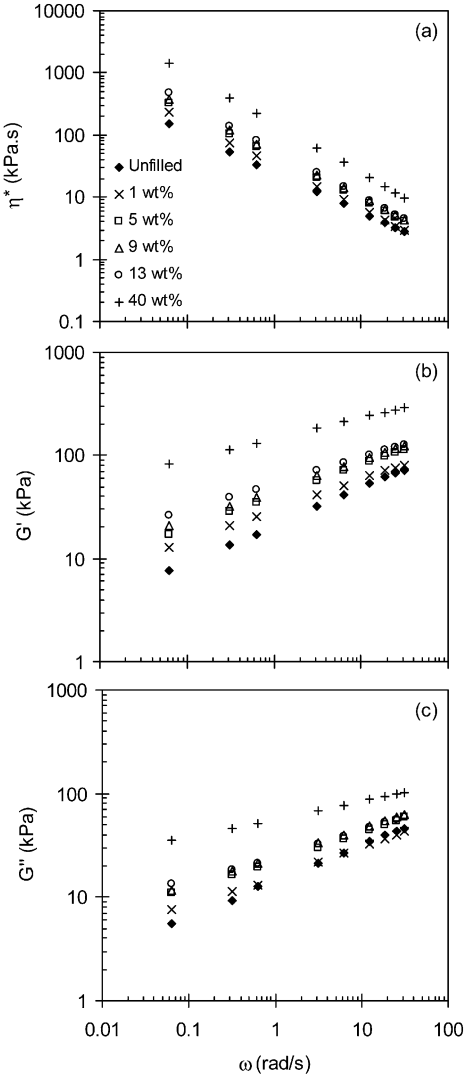

Fig. 6. (a) Complex viscosity (η^*), (b) elastic modulus (G'), and (c) viscous modulus (G'') as a function of frequency (ω) for the NR_4^+-MM/PE-*g*-PA composites at 150 °C.

The inspection of TEM images confirmed that NR_4^+-MM was efficiently exfoliated and dispersed within a polyampholyte matrix (Fig. 5(a)). In addition to revealing a high proportion of delaminated clay platelets, the images showed evidence of intercalated particles comprised of 2–4 silicate clay layers, whose disordered structure made them invisible to WAXS. The progressive exfoliation mechanism proposed by Dennis et al. [24] for the delamination and dispersion of organoclay is consistent with our WAXS and TEM observations of PE-*g*-PA composites. They have suggested that the application of shear to primary clay particles can result in their decomposition into smaller stacks comprised of 3–5 silicate platelets. Subsequent diffusion of polymer into the gallery spacing of the filler may compromise platelet ordering, while maintaining them in an aggregated state. As a result, clay aggregates may be transparent with respect to WAXS analysis, but observable in TEM images.

A better appreciation of the small-scale and disordered

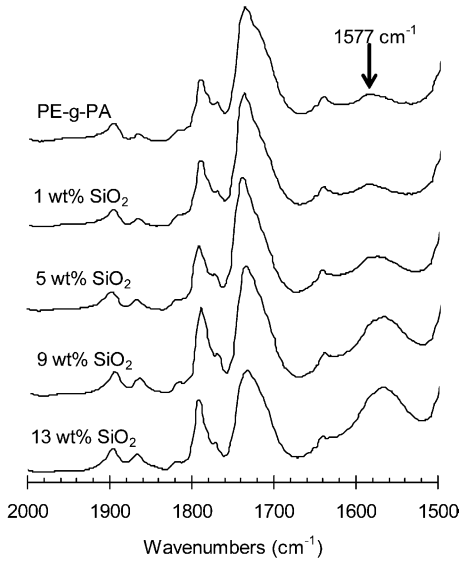

Fig. 7. FT-IR spectra of PE-*g*-PA and its SiO_2 composites.

structure of these intercalated aggregates is gained by comparing the polyampholyte nanocomposite with a corresponding material prepared from high-density polyethylene (HDPE). The latter composite is a conventional clay-filled system, since exfoliation cannot be achieved by unmodified polyethylene under these conditions. TEM analysis of this material revealed no individual clay platelets, only dense aggregates with micron-scale dimensions (Fig. 5(b)). The degree of clay exfoliation and dispersion shown in the PE-*g*-PA nanocomposite image (Fig. 5(a)) is all the more remarkable given that the material contains 40 wt% filler.

It is generally accepted that the high surface area of exfoliated NR_4^+-MM, combined with strong interactions at the polymer-filler interface, acts to immobilize polymer chains such that the melt viscosities are relatively high [8]. This applies to the ionomer of interest, since the introduction of exfoliated clay to PE-*g*-PA raised both the elasticity and the complex viscosity of the material (Fig. 6). These effects are not preferred outcomes from the perspective of polymer processing, but PE-*g*-PA and its nanocomposites display considerable shear-thinning behavior, which should facilitate processing at the high shear rates developed by standard equipment.

The effect of exfoliated clay on the mechanical properties of PE-*g*-PA is summarized by Table 1. Static tensile data reveal a significant positive effect on material stiffness that, unfortunately, is garnered at the expense of ductility, as the elongation at break dropped from 2190% in the unfilled system to 740% in a 9 wt% NR_4^+-MM composite.

3.4. Silica-ionomer composites

The challenge in producing silica nanocomposites is to achieve adequate filler dispersion. Unlike polyethylene, the surface energy of silica is comprised of a low dispersive component, and a high specific (polar) contribution [25]. This disparity encourages silica agglomeration into a secondary network of primary particles, whose formation opposes the objective of particle dispersion. Our interest in

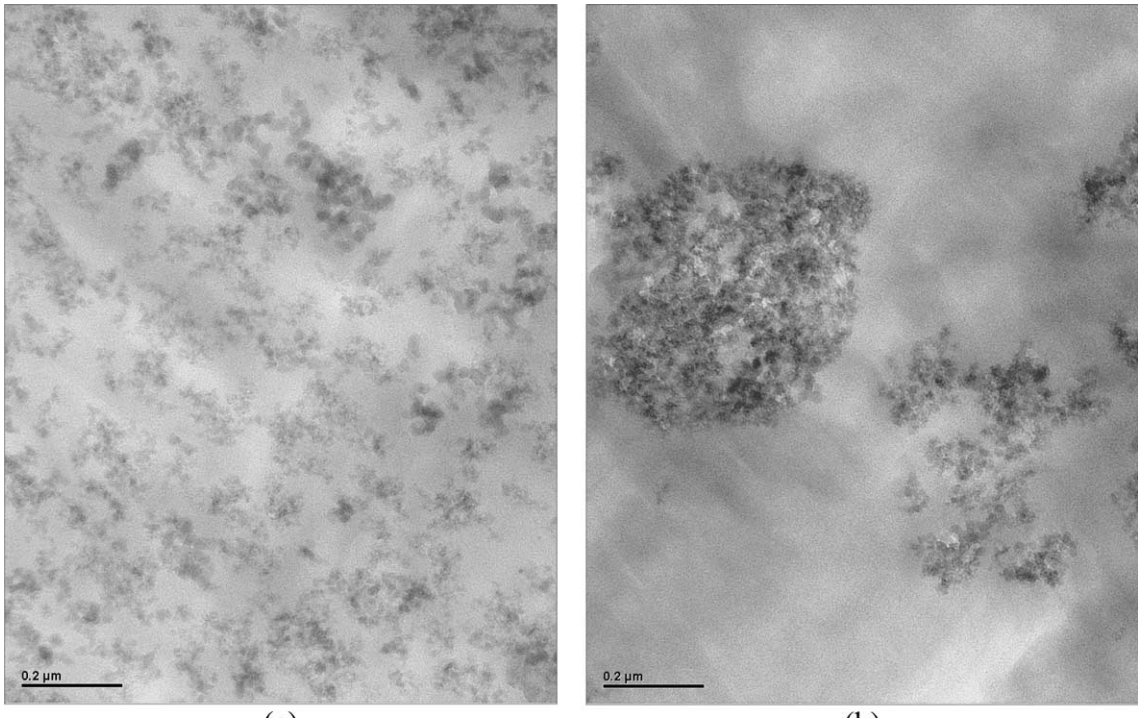

Fig. 8. TEM images of (a) 13 wt% SiO_2/PE-*g*-PA, (b) 5 wt% SiO_2/HDPE (scale bars correspond to 0.2 μm).

the silica/PE-*g*-PA system stemmed from the positive effects of ionic functionality on preparation of NR_4^+-MM-based composites. It was believed that ion–dipole associations between PE-*g*-PA and silica could alleviate differences in surface energy, thereby promoting filler dispersion and overall polymer reinforcement.

The premise that silica can interact with the ammonium carboxylate functionality within PE-*g*-PA has been validated by FT-IR analysis. The spectra presented in Fig. 7 show that the intensity of the $1577\ cm^{-1}$ resonance derived from the carboxylate anion increases in proportion to the silica content of the sample. The sensitivity of carboxylate anion resonances to hydrogen bonding environment is well established for small molecule systems, as well as in poly(ethylene-*co*-methacrylic acid) ionomers [26]. We suggest that growth of the $1577\ cm^{-1}$ resonance is due to hydrogen-bonding interactions between the acidic silanol functionality of filler surface with the carboxylate functionality of the polyampholyte. The significance of this observation lies in its demonstration of direct association between polyampholyte and nanofiller.

Fig. 8 shows TEM images of SiO_2 dispersed in PE-*g*-PA and a non-ionic HDPE material. Direct comparison of these images illustrates the superior filler dispersion provided by the polyampholyte. Whereas the unmodified HDPE composite contained large-scale particle agglomerates, even at relatively low SiO_2 contents, PE-*g*-PA yielded a fine network structure of remarkable uniformity. Although a small degree of silica agglomeration persisted in the polyampholyte nanocomposite, it is known that the strong tendency of unmodified silica to aggregate makes complete filler dispersion down to primary particles virtually unattainable, especially for non-polar matrices [18].

As expected, the compounding of nanosilica into PE-*g*-PA increased its melt viscosity and elasticity (Fig. 9). However, comparison of the NR_4^+-MM and SiO_2 composites show that on a weight basis, clay had greater influence in spite of the fact that NR_4^+-MM contains 40 wt% of tetraalkylammonium functionality. This effect is attributed to differences in specific surface area, since the large aspect ratio of exfoliated clay platelets creates a greater surface to volume ratio than that provided by spherical silica particles. It is interesting to note that such differences do not affect solid-state tensile properties, as revealed by the data summarized in Table 1. The SiO_2/PE-*g*-PA composites exhibited Young's moduli better than or equal to those recorded for comparable clay nanocomposites and they provided much better ductility. On this basis we conclude that nanosilica can provide a more favorable balance of melt viscosity, stiffness and failure properties when used in conjunction with PE-*g*-PA.

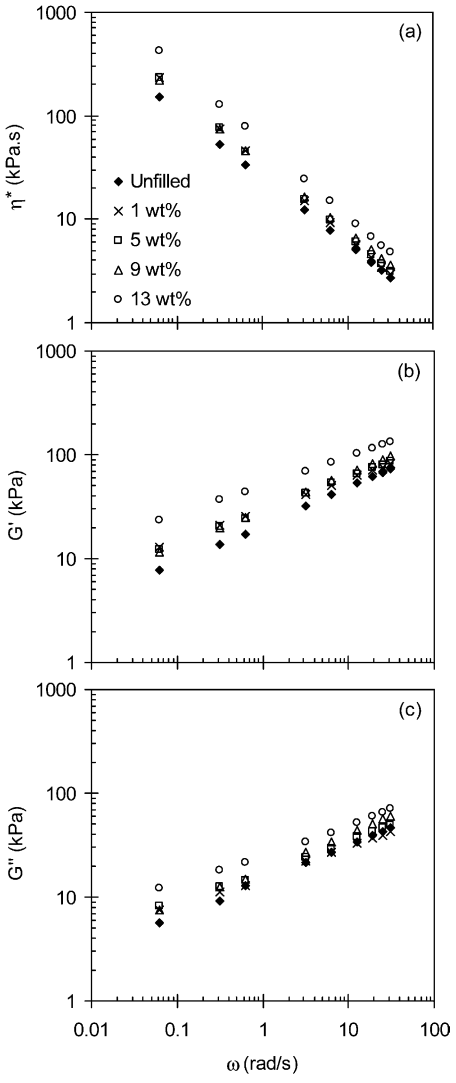

Fig. 9. (a) Complex viscosity (η^*), (b) elastic modulus (G'), and (c) viscous modulus (G'') as a function of frequency (ω) for the SiO_2/PE-*g*-PA composites at 150 °C.

Table 1
Tensile properties of PE-*g*-PA and its composites

Composition (wt% filler)	Young's modulus (MPa)	Yield stress (MPa)	Elongation at break (%)
NR_4^+-MM/PE-*g*-PA			
0	290±20	26±1	2190±340
1	320±10	25±1	1570±230
5	320±60	27±1	690±310
9	410±30	30±2	740±300
13	420±60	27±3	12±1
29	470±125	29±7	11±5
SiO_2/PE-*g*-PA			
0	30±10	26±1	2190±340
1	330±40	27±1	1150±380
5	340±20	28±1	1250±290
9	360±50	30±1	2010±360
13	400±50	31±2	1220±360

Values are reported with their 95% confidence interval.

4. Conclusions

A solvent-free reaction of maleated polyethylene with a tertiary amino alcohol yields an ammonium carboxylate polyampholyte, whose ionic functionality improves the clay exfoliation capacity of the polymer, and aids in the dispersion of nanosilica. Despite its relatively small surface area and its capacity to engage only in ion–dipole interactions with PE-*g*-PA, nanosilica provides a better balance of viscoelastic and mechanical properties when compared with onium-ion exchanged montmorillonite.

Acknowledgements

Financial support from the Natural Sciences and Engineering Research Council (NSERC) and Materials and Manufacturing Ontario (MMO)/Emerging Materials Knowledge (EMK) program is gratefully acknowledged. The authors wish to thank Nanocor Incorporated and Degussa Corporation for providing clay and silica samples, respectively, Mr Bob Whitehead of the Royal Military College (RMC) for WAXS analysis, and Mr Doug Holmyard of Mount Sinai Hospital for TEM testing. The authors are indebted to Professor Chul Park of the University of Toronto for contributing the TEM image of the NR_4^+-MM/HDPE composite.

References

[1] Sakamoto K, MacKnight WJ, Porter RS. J Polym Sci 1970;8:277–87.
[2] Earnest Jr TR, MacKnight WJ. J Polym Sci, Polym Phys Ed 1978;16:143–57.
[3] Bonotto S, Bonner EF. Macromolecules 1968;1(6):510–5.
[4] Tobolsky AV, Lyons PF, Hata N. Macromolecules 1968;1(6):515–9.
[5] Eisenberg A, Navratil M. Macromolecules 1974;7(1):90–4.
[6] Weiss RA, Fitzgerald JJ, Kim D. Macromolecules 1991;24(5):1071–6.
[7] Lundberg RD, Makowski HS. J Polym Sci, Polym Phys Ed 1980;18:1821–36.
[8] Chisholm BJ, Moore RB, Barber G, Khouri F, Hempstead A, Larsen M, et al. Macromolecules 2002;35(14):5508–16.
[9] Parent JS, Liskova A, Resendes R. Polymer 2004;45(24):8091–6.
[10] Gopakumar TG, Lee JA, Kontopoulou M, Parent JS. Polymer 2002;43(20):5483–91.
[11] Lee JA, Kontopoulou M, Parent JS. Polymer 2004;45(19):6595–600.
[12] Wang KH, Choi MH, Koo CM, Choi YS, Chung IJ. Polymer 2001;42(24):9819–26.
[13] Hotta S, Paul DR. Polymer 2004;45(22):7639–54.
[14] Kawasumi M, Hasegawa N, Kato M, Usuki A, Okada A. Macromolecules 1997;30(20):6333–8.
[15] Galgali G, Ramesh C, Lele A. Macromolecules 2001;34(4):852–8.
[16] Solomon MJ, Almusallam AS, Seefeldt KF, Somwangthanaroj A, Varadan P. Macromolecules 2001;34(6):1864–72.
[17] Marchant D, Jayaraman K. Ind Eng Chem Res 2002;41(25):6402–8.
[18] Wang M-J. Rubber Chem Techol 1998;71(3):520–89.
[19] Mavridis H, Shroff RN. Polym Eng Sci 1992;32(23):1778–91.
[20] Wang Y, Ji D, Yang C, Zhang H, Qin C, Huang B. J Appl Polym Sci 1994;52(10):1411–7.
[21] Brozoski BA, Painter PC, Coleman MM. Macromolecules 1984;17(8):1591–4.
[22] Ferry JD. Viscoelastic properties of polymers. New York: Wiley; 1980.
[23] Eisenberg A, Navratil M. Macromolecules 1973;6(4):604–12.
[24] Dennis HR, Hunter DL, Chang D, Kim S, White JL, Cho JW, et al. Polymer 2001;42(23):9513–22.
[25] Wang M-J, Wolff S. Rubber Chem Technol 1992;65(4):715–35.
[26] Coleman MM, Lee JY, Painter PC. Macromolecules 1990;23(8):2339–45.